

UVIT view of ram-pressure stripping in action: Star formation in the stripped gas of the GASP jellyfish galaxy JO201 in Abell 85

K. George^{1,★}, B. M. Poggianti², M. Gullieuszik², G. Fasano², C. Bellhouse^{4,3}, J. Postma⁵, A. Moretti², Y. Jaffé³, B. Vulcani^{6,2}, D. Bettoni², J. Fritz⁷, P. Côté⁸, S. K. Ghosh^{9,10}, J. B. Hutchings⁸, R. Mohan¹, P. Sreekumar¹, C. S. Stalin¹, A. Subramaniam¹, S.N. Tandon^{1,11}

¹Indian Institute of Astrophysics, Koramangala II Block, Bangalore, India

²INAF-Astronomical Observatory of Padova vicolo dell'Osservatorio 5 35122 Padova, Italy

³European Southern Observatory, Alonso de Cordova 3107, Vitacura, Casilla 19001, Santiago de Chile, Chile

⁴University of Birmingham School of Physics and Astronomy, Edgbaston, Birmingham, England

⁵University of Calgary, Calgary, Alberta, Canada

⁶School of Physics, The University of Melbourne, Swanston St & Tin Alley Parkville, VIC 3010, Australia

⁷Instituto de Radioastronomía y Astrofísica, UNAM, Campus Morelia, A.P. 3-72, C.P. 58089, Mexico

⁸National Research Council of Canada, Herzberg Astronomy and Astrophysics Research Centre, Victoria, Canada

⁹National Centre for Radio Astrophysics, Pune, India

¹⁰Tata Institute of Fundamental Research, Mumbai, India

¹¹Inter-University Center for Astronomy and Astrophysics, Pune, India

Accepted XXX. Received YYY; in original form ZZZ

ABSTRACT

We report the ultraviolet (UV) imaging observation of a jellyfish galaxy obtained at high spatial resolution (1.3-to-1.5 Kpc) using the Ultra Violet Imaging Telescope on board ASTROSAT. Jellyfish galaxies observed in galaxy clusters are subjected to strong ram-pressure effects that strip the gas from the galaxy. The $H\alpha$ images of jellyfish galaxies reveal tails of ionized gas extending up to 100 Kpc , which could be hosting ongoing star formation. The star formation in the tentacles of the jellyfish galaxy JO201 in the Abell 85 galaxy cluster at redshift ~ 0.056 is directly studied from near ultraviolet (NUV) and far ultraviolet (FUV) imaging observations. The intense burst of star formation happening in the tentacles is the focus of the present study. JO201 is the "UV-brightest cluster galaxy" in Abell 85 with knots and streams of star formation in the ultraviolet. We identify the star forming knots both in the stripped gas and in the galaxy disk and compare the features seen in UV with the ones traced by $H\alpha$ emission from data cubes taken as part of the GASP program using MUSE on the VLT. The UV and $H\alpha$ emission in main body and along the tentacles of JO201 show a remarkable correlation. We created the FUV extinction map of JO201 using the $H\alpha$ and $H\beta$ flux ratio. The star formation rates of individual knots are derived from the extinction corrected FUV emission, which agree very well with those derived from the $H\alpha$ emission, and range from ~ 0.01 -to- $2.07 M_{\odot} yr^{-1}$. The integrated star formation rate from FUV flux (SFR_{FUV}) is about $\sim 15 M_{\odot}/yr$, which is rather typical for star forming galaxies of this mass in the local Universe. We demonstrate that the unprecedented deep UV imaging study of the jellyfish galaxy JO201 show clear sign of extraplanar star-formation activity, resulting from a recent/ongoing gas stripping event.

Key words: galaxies: clusters: intracluster medium, galaxies: star formation

1 INTRODUCTION

Galaxies in the local Universe follow a bimodal distribution in the optical color-magnitude diagram with a red sequence

★ E-mail: koshy@iiap.res.in

populated by old, red galaxies and a blue cloud with young actively star-forming blue galaxies (Visvanathan & Sandage 1977; Baldry et al. 2004). Galaxies on the red sequence are mostly of early-type (E/S0) morphology and host little cold gas and dust, whereas galaxies on the blue cloud have late-type (spirals) morphology and usually host an abundant cold gas content. A significant fraction of red sequence galaxies are observed to be located in the densest regions of the local Universe like the cores of massive galaxy clusters. The blue cloud galaxies are found mostly in the low density regions of the Universe, i.e. in the field environment, as well as in cluster outskirts.

The change in the morphology and the star formation properties of galaxies with changing galaxy density is now believed to be influenced by the rapid decline in star formation as galaxies fall into the dense cluster environment from the field. The morphology-density relation, the Butcher-Oemler effect and the high occurrence of blue star-forming galaxies in the cluster outskirts are the observational support for this galaxy transformation in dense environments. (Dressler 1980; Butcher & Oemler 1984; Oemler et al. 2009; Mahajan et al. 2012; Fasano et al. 2015). There are multiple processes, such as strangulation, harassment and ram pressure stripping, which can act alone or in combination to convert a star-forming galaxy into a non star-forming one when they experience the cluster environment.

Ram pressure is the main mechanism in quenching star formation in cluster galaxies. The intra-cluster medium is composed of hot X-ray emitting plasma with temperatures in the range $10^7 - 10^8$ K and electron density in the range $10^{-4} - 10^{-2} \text{ cm}^{-3}$ contained in a region of typical size 2 Mpc (Sarazin 1986; Fabian 1994). When a galaxy falls into the intra-cluster medium, its interstellar medium interacts with a force in the opposite direction of the relative motion. The cold gas gets stripped from the disk of the fast moving spiral galaxies through the process of ram pressure stripping (Gunn & Gott 1972). The in-falling gas rich spiral galaxies thus go through a phase of morphological transformation, partly or even fully due to gas removal processes. The stripping of gas quenches the star formation and transforms the galaxies into passively evolving red sequence systems (Dressler et al. 1997; Poggianti et al. 1999; Dressler et al. 2013).

Gas-rich spiral galaxies have spatially extended loose gas halos and tightly bound disk gas, both of which are subjected to the harsh impact of cluster in-fall (Bekki 2009). The observations and simulations of in-falling galaxies have given ample evidence for the presence of stripped neutral and molecular hydrogen in the opposite direction to the velocity vector. (Haynes et al. 1984; Cayatte et al. 1990; Kenney et al. 2004; Chung et al. 2009; Vollmer et al. 2001; Serra et al. 2013; Jaffé et al. 2015; Yoon et al. 2017; Tonnesen & Bryan 2009, 2012; Jáchym et al. 2014; Verdugo et al. 2015; Jáchym et al. 2017) (Moretti et al. in preparation). The gas gets stripped but also shock compressed, and this can trigger pockets of intense star formation. Galaxies undergoing strong ram-pressure events can sometimes be identified in optical observations due

Table 1. Log of UVIT observations of Abell 85 galaxy cluster.

Channel	Filter	$\lambda_{mean}(\text{\AA})$	$\delta\lambda(\text{\AA})$	Int:time(s)
FUV	F148W	1481	500	15429
NUV	N242W	2418	785	18326

to the existence of tentacles of debris material resembling a jellyfish. The optical and H α observations of galaxies falling into nearby galaxy clusters have shown disturbed H α emission with undisturbed stellar disks (Kenney & Koopmann 1999; Yoshida et al. 2008; Hester et al. 2010; Kenney et al. 2014). The triggered star formation in the stripped gas appear as tentacles and give the galaxy a visual appearance of jellyfish morphology (Owen et al. 2006; Cortese et al. 2007; Owers et al. 2012; Fumagalli et al. 2014; Ebeling et al. 2014; Rawle et al. 2014; Poggianti et al. 2016; Bellhouse et al. 2017; Gullieuszik et al. 2017). Star formation happening in the compressed gas within the galaxy and in the ejected gas makes these galaxies bright in the ultraviolet. Young, massive stars (O,B,A spectral types) emit the bulk of radiation in the ultraviolet (UV) region of the spectral energy distribution and hence UV can be used as a direct probe to study ongoing star formation. The nature of the intense star formation in the main body of the galaxy and the debris material of the jellyfish galaxies can thus be directly studied using ultraviolet observations.

We present here the ultraviolet study of the jellyfish galaxy JO201 undergoing extreme ram-pressure stripping in the massive galaxy cluster Abell 85. *The aim of the present study is to identify the sites of intense star formation in the stripped gas and in the galaxy disk and estimate the star formation rates.* JO201 is taken from the sample of 419 (344 cluster and 75 field) jellyfish candidates of Poggianti et al. (2016) and is one of the most striking cases of ram-pressure stripping in action (see (Bellhouse et al. 2017; Poggianti et al. 2017; Jaffe' et al. 2018)). The galaxy has a spiral morphology with tails of material to one side in the optical images and total stellar mass $\sim 6 \times 10^{10} M_{\odot}$ for a Salpeter IMF between 0.1 and $100 M_{\odot}$ (Bellhouse et al. 2017; Salpeter 1955). (The total stellar mass is computed for a Chabrier IMF in Bellhouse et al. (2017)). Here we compute the value for a Salpeter IMF). The galaxy is falling into the cluster from the back with a slight inclination from the line-of-sight directed to the west: this explains the jellyfish morphology with projected tails pointing towards the east, in the direction of the brightest cluster galaxy (BCG). In what follows we compare the UV and H α emission across JO201. We discuss the observations in section 2, and present the results in section 3. We summarize the key findings from the study in section 4. Throughout this paper we adopt a Salpeter 0.1- $100 M_{\odot}$ initial mass function, and a concordance Λ CDM cosmology with $H_0 = 70 \text{ km s}^{-1} \text{ Mpc}^{-1}$, $\Omega_M = 0.3$, $\Omega_{\Lambda} = 0.7$.

2 OBSERVATIONS, DATA & ANALYSIS

The galaxy JO201 was observed at optical wavelengths as part of the WINGS and OmegaWINGS surveys (Fasano et al. 2006; Gullieuszik et al. 2015; Moretti et al. 2017) and

with MUSE on the VLT under the programme GASP (Gas Stripping Phenomena in galaxies with MUSE) aimed at investigating the gas removal process in galaxies using the spatially resolved integral field unit spectrograph MUSE (Poggianti et al. 2017; Bellhouse et al. 2017). JO201 (RA: 00:41:30.325, Dec: - 09:15:45.96) belongs to the massive galaxy cluster Abell 85 ($M_{200} = 1.58 \times 10^{15} M_{\odot}$) at a redshift ~ 0.056 (Moretti et al. 2017). The corresponding luminosity distance is ~ 250 Mpc and the angular scale of $1''$ on the sky corresponds to 1.087 kpc at the galaxy cluster rest frame.

The jellyfish galaxy JO201 was observed with the ultra-violet imaging telescope (UVIT) onboard the Indian multi wavelength astronomy satellite ASTROSAT (Agrawal 2006). The UVIT consists of twin telescopes, a FUV (130-180nm) telescope and a NUV (200-300nm), VIS (320-550nm) telescope which operates with a dichroic beam splitter. The telescopes are of 38cm diameter and generate circular images over a $28'$ diameter field simultaneously in all three channels (Kumar et al. 2012). There are options for a set of narrow and broad band filters, out of which we used the NUV N242W and FUV F148W filters for NUV and FUV imaging observations. Table 1 gives details on the UVIT observations of the Abell 85 galaxy cluster. We note that there are GALEX observations of JO201 with an integration time of 25ks in NUV and 2.5ks in FUV channel (also see Venkatapathy et al. (2017)). The UVIT observations for JO201 is at an angular resolution of $\sim 1''.2$ for the NUV and $\sim 1''.4$ for the FUV channels, while the GALEX resolution is $\sim 4-5$ arcsec¹ (Subramaniam et al. 2016; Tandon et al. 2016). The NUV and FUV images are corrected for distortion (Girish et al. 2017), flat field and satellite drift using the software CCDLAB (Postma & Leahy 2017). The images from 10 orbits are coadded to create the master image. The astrometric calibration is performed using the `astrometry.net` package where solutions are performed using USNO-B catalog (Lang et al. 2010). The photometric calibration is done using the zero point values generated for photometric calibration stars as described in Tandon et al. (2017).

Abell 85 galaxy cluster imaging observations in the B and V bands were taken as part of the WINGS survey (Varela et al. 2009) and the galaxy JO201 was observed with the MUSE integral-field spectrograph mounted on the ESO Very large Telescope as part of the GASP program, with photometric conditions and image quality of $\sim 0''.7$ FWHM, as described in detail in Bellhouse et al. (2017). MUSE has a $1' \times 1'$ field of view and JO201 was covered with two MUSE pointings. The MUSE observations cover the stripped tails of the galaxy and confirm that JO201 is indeed a jellyfish galaxy undergoing intense ram-pressure stripping by the intra-cluster medium, close to the core of the massive cluster Abell 85. These data reveal extended $H\alpha$ emission out to ~ 60 kpc from the stellar disk of the galaxy with kinematics indicative of significant stripping in the line-of-sight direction (Bellhouse et al. 2017). The $H\alpha$ emission line flux map of JO201 from MUSE (which we call $H\alpha$ image as de-

scribed in Bellhouse et al. (2017)) is used in this study for comparison with UV imaging data. We extracted a region around JO201 from the NUV and FUV images and recentered the astrometric solution to match point sources from WINGS catalog. The UV and $H\alpha$ images are then assigned to the same astrometric reference frame with an accuracy better than $1''$. A color composite image of the Abell 85 cluster central region including both JO201 and the Brightest Cluster Galaxy created using NUV, B and V band images is shown in Figure 1. The red and green colors correspond to the flux from the B and V images from the WINGS survey and the NUV image from UVIT is shown in blue color.

3 RESULTS

3.1 Ultraviolet imaging

The UVIT $28'$ field of view corresponds to ~ 1.83 Mpc at the Abell 85 galaxy cluster rest frame. The NUV image is having higher angular resolution compared to FUV image and therefore we use the NUV image to identify star forming regions in JO201. We show the NUV image of a region centered on the jellyfish galaxy JO201 in Figure 2. The NUV image is clearly showing a wealth of information, which include low surface brightness features outside of the galaxy disk, knots on the galaxy disk and knots outside of the galaxy in the intergalactic space that seem to follow the spiral pattern from the galaxy disk (see Fig. 8 in Bellhouse et al. (2017)), possibly suggesting unwinding of spiral arms. The NUV emission from the main body and the tentacles of JO201 appears to be clumpy in nature with knots having flux due to emission from star formation. The bright source at the center of JO201 corresponds to the AGN identified by Poggianti et al. (2017) (see also Bellhouse et al. in prep). The FUV image displays similar morphological features to the NUV image but since the NUV image has a better signal to noise ratio and resolution compared to the FUV image, we used the NUV image to first identify the knots and quantify the flux within the detected knots.

3.2 Combining Ultraviolet and $H\alpha$

The UV emission is coming from young, massive hot stars (OBA spectral types) on the main sequence and hence is a direct probe of recent star formation in the tentacles of JO201. While the stellar mass range probed by the UV is typically $M_{\star} > 5 M_{\odot}$, with stellar lifetimes of 200 Myr or less, the $H\alpha$ emission in star-forming regions is due to the recombination of hydrogen that is ionized by stars in the range $M_{\star} > 20 M_{\odot}$, (O & B spectral type) whose lifetimes are 10-20 Myr or shorter (Kennicutt 1998; Kennicutt & Evans 2012). $H\alpha$ and UV emission therefore probe different star formation timescales. The UV flux from the knots can thus have contributions from single or multiple bursts or prolonged star formation during the past few 10^8 yr, while the $H\alpha$ flux derives from the current "ongoing" star formation. Moreover, the $H\alpha$ emission originates from the gas and therefore is an indirect tracer of ongoing star formation, while the UV probes directly the light coming from young stellar photospheres.

¹ UVIT NUV N242W and FUV F148W filters have similar band-pass to GALEX NUV and FUV filters.

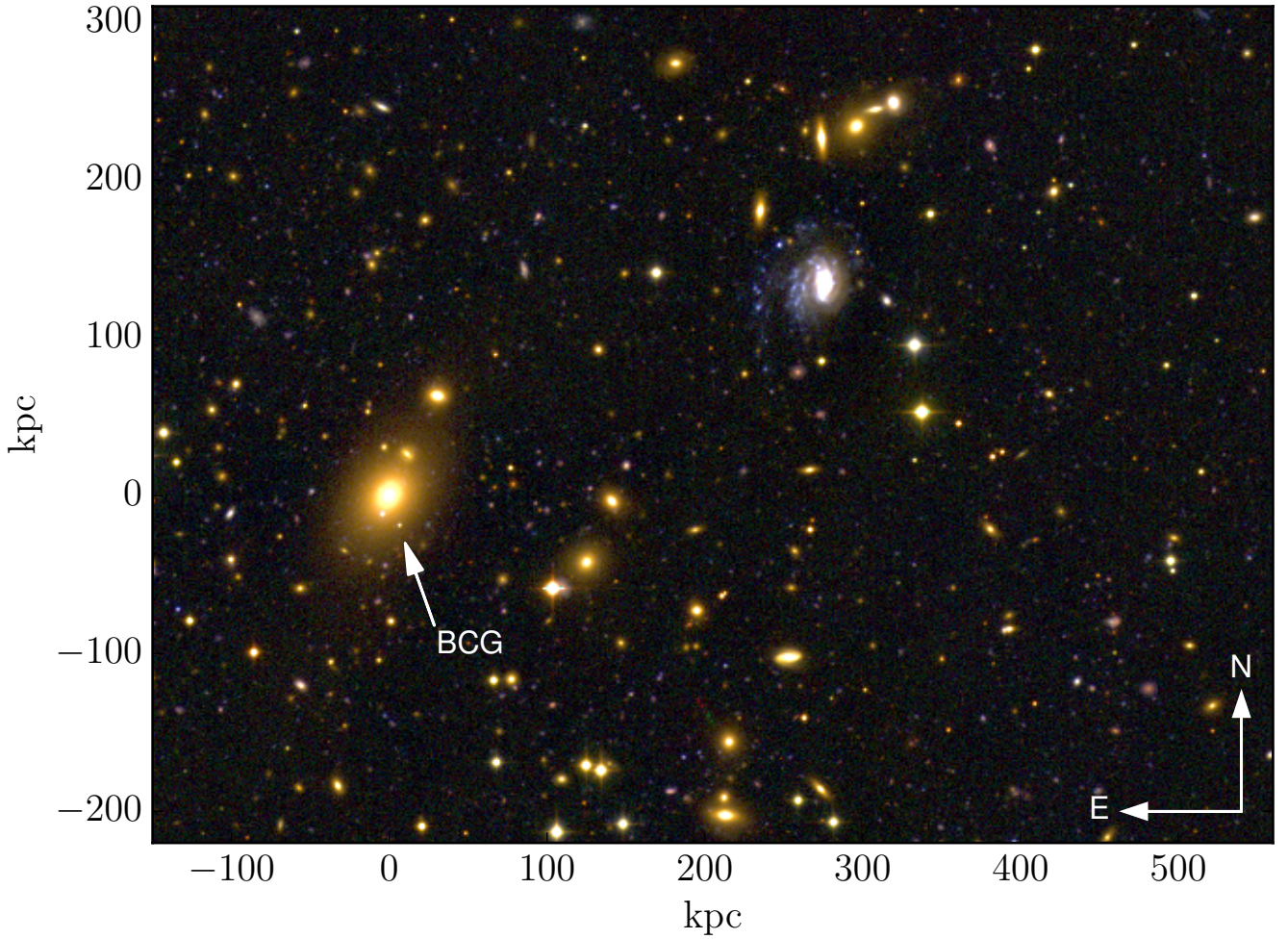


Figure 1. Color-composite image of the Abell 85 galaxy cluster field. The image is made from combining NUV (colored blue) and optical *B*, *V* filter band pass images. The jellyfish galaxy is prominent in NUV as evident from the enhanced blue color from JO201. The position of the brightest cluster galaxy (BCG) is shown. The image is of size $\sim 12.0' \times 8.0'$.

In principle, interstellar shocks can also be responsible for generating UV radiation (Shull & McKee 1979) and hence the UV emission from the stripped gas of JO201 can have a shock component. The MUSE data show that the radiation ionizing the gas throughout the disk and in the tails (except in the central region of the galaxy powered by the AGN (Poggianti et al. 2017)) has emission-line ratios typical of ionizing radiation from young host stars (Bellhouse in prep.). Hence, it is reasonable to assume that the UV fluxes we observe with UVIT are dominated by young stellar light. Note that the contribution of evolved population of metal poor extreme horizontal branch stars from the disk of the galaxy can contaminate the UV flux from the young stars, but this is expected to be negligible in the presence of strong ongoing star formation as in JO201. We stress that we are not using the UV flux from the central region of the galaxy in the present study as it is contaminated by the contribution from AGN. As we will show later, the star-forming origin of the UV emission in JO201 is also corroborated by the good agreement found using $H\alpha$ and UV as independent star formation indicators.

We compared the NUV and FUV images of JO201 against the $H\alpha$ image in the following. The main motivation is to probe common features and also check for any missing features between the images. We again note that the NUV/FUV flux probe star forming region with ages < 200 Myr, whereas the $H\alpha$ flux is coming from star formation ages < 20 Myr. We compare the NUV and the $H\alpha$ emission in Figure 3. We note that the MUSE plate scale is $0.2''/\text{pixel}$ with resolution $\sim 0.7''$ whereas the UVIT plate scale is $0.4''/\text{pixel}$ with resolution of $1.2''$ in the region of the galaxy. The image scaling is set such that the pixels corresponding to the brightest regions on both images are highlighted. The $H\alpha$ and NUV combined image analysis of Figure 3 shows a number of characteristics. We note that many features seen in the $H\alpha$ image are also seen in NUV image. There is generally a good coincidence of NUV and $H\alpha$ regions corresponding to peaks of star formation both in the stripped gas and on the disk of the galaxy.

The $H\alpha$ contours corresponding to JO201 from the MUSE imaging data is overlaid over the FUV image in Figure 4. It is interesting to note that the FUV emission is showing

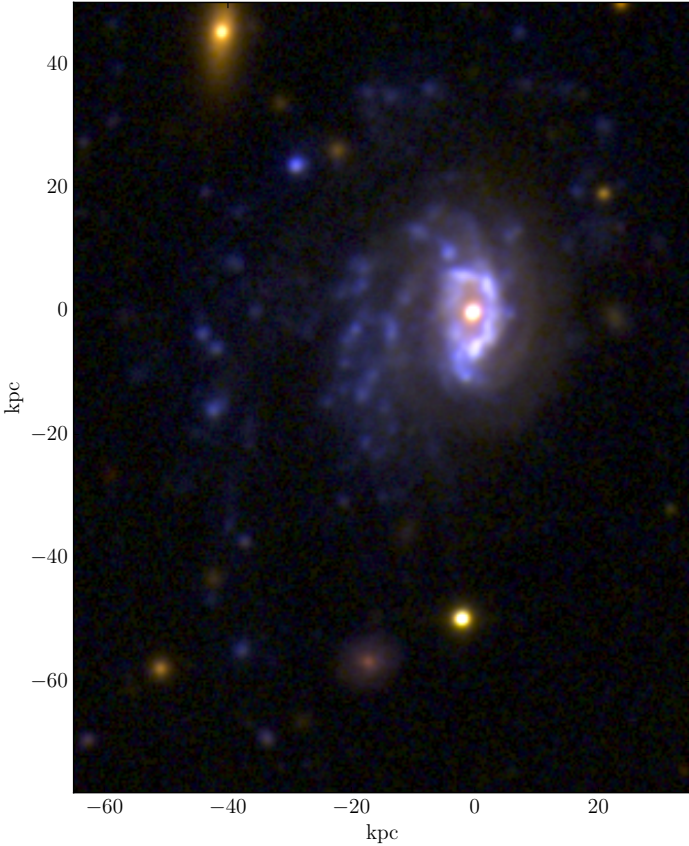


Figure 2. The NUV and optical composite image of JO201. The image is made from combining NUV (colored blue) and optical B, V filter band pass images. Note the diffuse emission and the knots of star formation in the stripped material from the galaxy. The bright source at the center is powered by an active galactic nucleus.

a remarkable coincidence with the $H\alpha$ regions and the detected flux from both images are having a common source of origin, which is ongoing star formation. There are few $H\alpha$ contours (star forming knots) with no significant flux in FUV image. This may be below the detection limit for UVIT or alternatively relatively young stars (<10 Myrs) contributing to the $H\alpha$ flux.

3.3 Star forming knots

The NUV knots are detected using a customized code in IRAF and FORTRAN, as described in Poggianti et al. (2017). The centers of NUV knot candidates are first identified as local minima onto the laplace +median filtered NUV image (IRAF-laplace and IRAF-median tools). A "robustness index" is then associated with each local minimum, based on the gradient concordance toward the knot center for pixels around the minimum. The final catalog of knot positions includes the local minima whose robustness index exceeds a given value. In the second step, the knot radii are estimated from the original NUV image, and their photometry is performed by a purposely devised FORTRAN code. In particular, the knots' radii are estimated through a recursive (outward) analysis of three at a time, consecu-

tive circular shells (thickness: one pixel) around each knot center. The iteration stops and the knot radius is recorded when at least one of the following circumstances occurs for the current outermost shell: (a) the counts of at least one pixel exceed those of the central pixel; (b) the fraction of pixels with counts greater than the average counts of the preceding shell ("bad" pixels) exceeds a given maximum value ($1/3$); (c) the average counts of "good" (not "bad") pixels are lower than a given threshold value, previously set for the diffuse emission; and (d) the image edges are reached by at least one pixel. The knot radii provided in this way are used to obtain, for each knot, the total counts inside the circle defining the knot, both including and excluding the counts below the threshold previously set for the diffuse emission (counts of pixels belonging to different knots are equally shared among them). Besides the centers and the above mentioned measures for each knot, the final catalog associated with NUV image provides a number of useful global photometric quantities of the NUV image, including: (a) total counts coming from the knots according to the three measures described above; (b) total counts attributable to the diffuse emission, both including and excluding the pixels inside the knot circles; and (c) total counts of pixels with counts above the diffuse emission threshold but lying outside the knot circles. The code was first run on the NUV image and we detected 89 knots of varying radii associated with the stellar disk and the tentacles on the NUV image of JO201. The MUSE data cover 85 of these knots. In principle, there can be background/foreground objects contaminating our bonafide knots belonging to JO201. In the following we will use the redshift provided by the MUSE spectra at each location to confirm that these knots indeed belong to JO201. Figure 5 shows the detected knots (in red) overlaid over the NUV image of JO201. We used the position and radius of these knots to measure the flux from both the NUV and the FUV images and the $H\alpha$ image. NUV magnitudes are computed for the knots and are shown in Figure 6.

The star formation in the knots outside the disk of JO201 can be interpreted as in-situ newly born stars from the ram-pressure stripped gas. Slightly older stars could be decoupled from the natal gas cloud and hence the UV (which directly traces < 200 Myr stars) and $H\alpha$ (tracing < 10 Myr stars) emission could have an offset, as described for example in Kenney et al. (2014) for the jellyfish galaxy IC3418 in the Virgo cluster. We checked for any offset between the UV and $H\alpha$ peak emission within the knots of JO201. The knot detecting algorithm was independently run on NUV and $H\alpha$ images. We demonstrate in Figure 7 the relative offset (red color for NUV knots and blue color for $H\alpha$ knots) between the knots detected from NUV image and the knots detected from $H\alpha$ image. We found that the peak emission from the knots match within the instrument resolution of the images. This is somehow expected for JO201, since the galaxy is moving mostly in the direction of the observer and therefore any positional offset between the UV and $H\alpha$ peaks would be hard to detect in projection.

The size distribution of the knots detected from NUV imaging is shown in Figure 8. The detected knots are of varying radius over 1.4 -to- 4.9 Kpc. We note that the lower limit is set by the resolution of the NUV image, hence most of the UV knots might be in fact unresolved. Anyhow, for those that are resolved, we can conclude that the star-forming re-

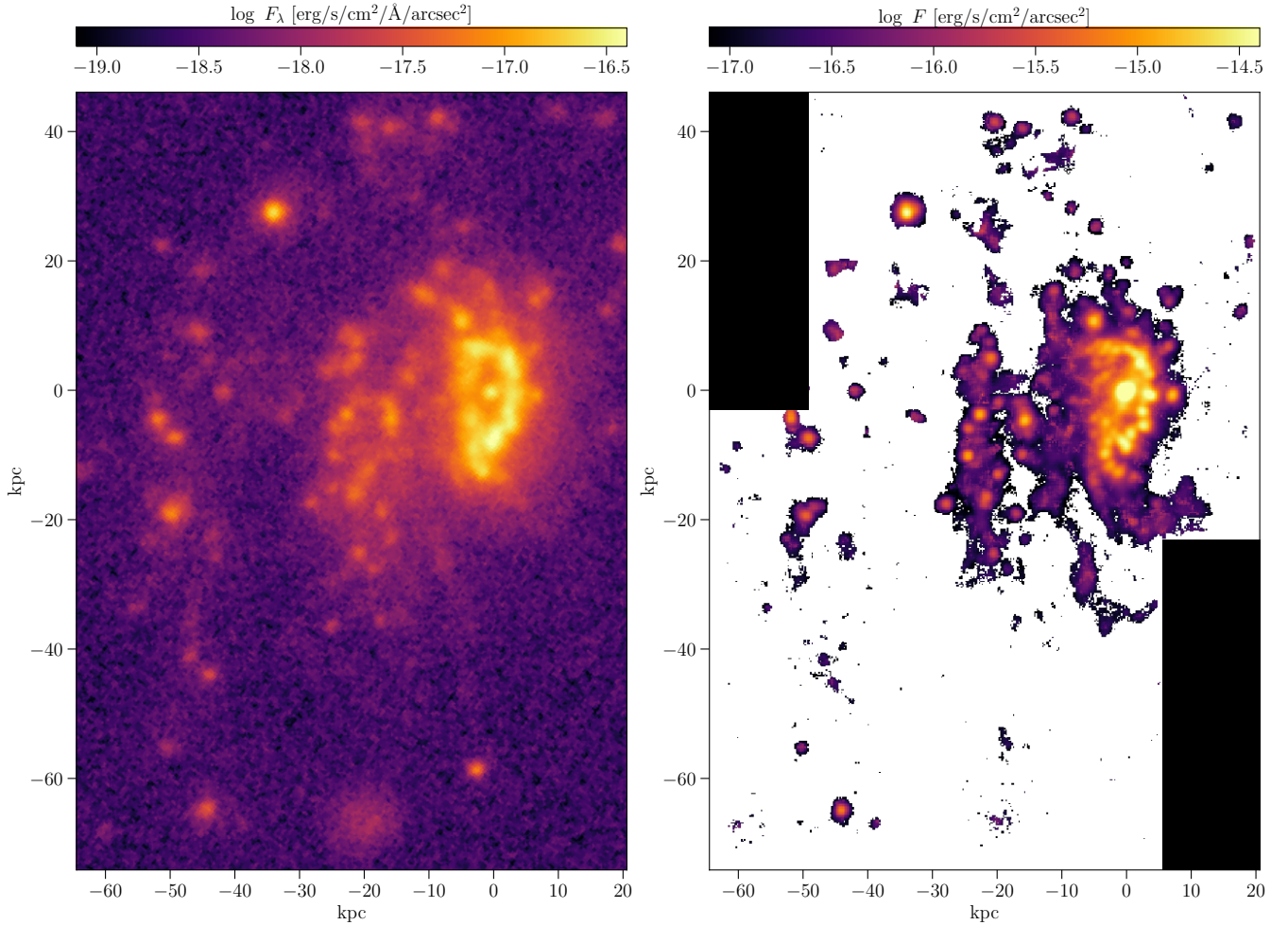


Figure 3. NUV (left) and $H\alpha$ (right) image of JO201 with the same spatial scale and with a flux scaling that allows to bring out the the brightest pixels. The NUV image covers a larger field compared to the dust corrected $H\alpha$ image.

gions identified in the UV images can be as large as a ~ 5 Kpc in radius.

3.4 Ultraviolet Extinction correction

To obtain the intrinsic UV fluxes of each knot from the observed fluxes we need to correct for extinction from dust both in our own Milky Way along the line of sight and within JO201. This is needed since star-forming regions are associated with significant amount of dust and the ultraviolet radiation is strongly affected by dust extinction. We use the FUV flux to estimate the star formation rate in the following section and hence correct the FUV flux for extinction. We first corrected the observed FUV flux for Galactic extinction ($A_V=0.0987$ in the direction of JO201) applying the Cardelli extinction law (Cardelli et al. 1989). We then corrected the observed FUV flux for rest frame extinction with the following method. We used the ratio of the $H\alpha$ and $H\beta$ emission line fluxes obtained from the MUSE data (Balmer decrement) assuming an intrinsic $H\alpha/H\beta=2.86$ and the Cardelli law to correct the $H\alpha$ flux at each location (i.e. MUSE spaxel). From the comparison between the total $H\alpha$ flux corrected and uncorrected for dust within each knot we

computed the global $A_{H\alpha}$ correction for each knot. According to the attenuation law from Calzetti et al. (2000), the ratio between the extinction at the FUV $A_{\lambda=1481}$ and $A_{H\alpha}$ is equal to 1.38, therefore we used the appropriate value of $1.38 \times A_{H\alpha}$ for each knot to correct the FUV flux. For those few knots which happen to fall outside of the MUSE field of view we could not apply any dust correction. Of the 85 UV knots which cover the footprint of the MUSE observations of JO201, 80 are confirmed based on redshift information as associated with JO201 and have a reliable estimate of $A_{H\alpha}$. The FUV extinction values (A_{FUV}) of these 80 knots are shown in Figure 9.

3.5 Star formation rates

The dust-corrected FUV flux can be used to compute the star formation rate of star forming regions assuming a constant star formation rate over the past 10^8 years. The star formation rate along the tentacles and the disk of JO201 is computed for a Salpeter initial mass function from the FUV luminosity (L_{FUV}) (Kennicutt 1998). We used the following form of equation as described in Iglesias-Páramo et al. (2006) and adopted in Cortese et al. (2008) to compute the

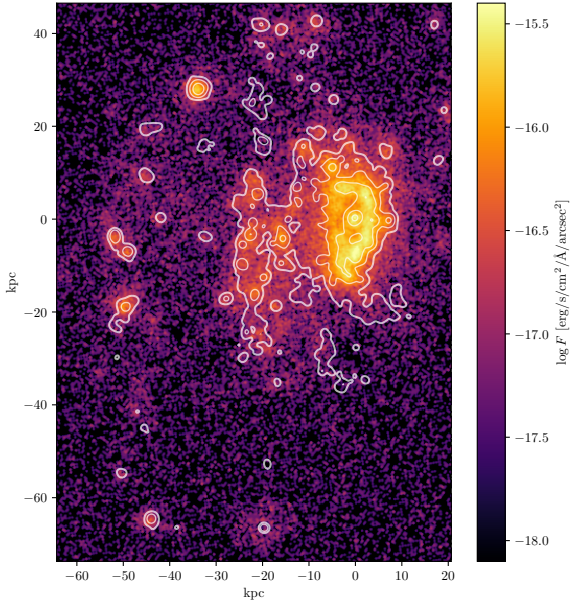


Figure 4. The flux contours generated from the MUSE H α image is overlaid over the FUV image of JO201.

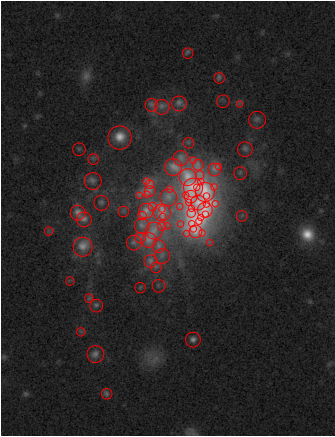


Figure 5. The NUV grey scale image of JO201. The red circles indicate the 89 knots identified with the procedure described in the text.

star formation rate from FUV flux of the detected knots. Note that the formula is derived using *Starburst99* synthesis model (Leitherer et al. 1999) for solar metallicity and a Salpeter 0.1-100 M_{\odot} initial mass function.

$$SFR_{FUV}[M_{\odot}/yr] = \frac{L_{FUV}[erg/sec]}{3.83 \times 10^{33}} \times 10^{-9.51} \quad (1)$$

The sky projected position diagram of star formation rate of the knots is shown in Figure 10 and the distribution

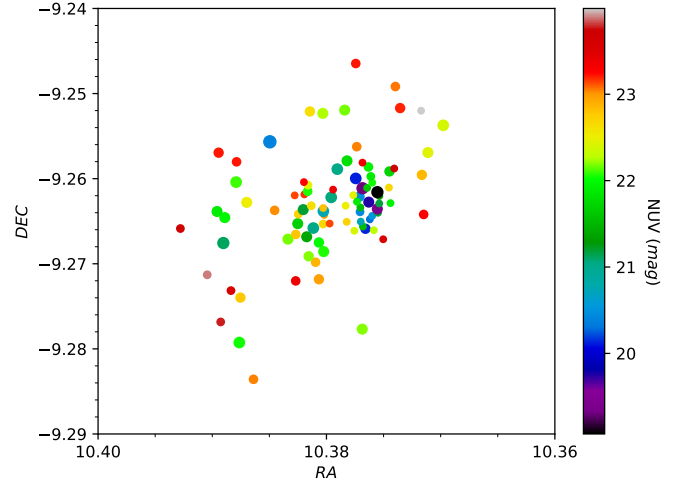


Figure 6. The distribution on the sky of the detected knots with color-coded observed NUV magnitude. The scaling is shown in the color bar. The size of the point is proportional to the radius of the knot. Note the central bright knot, which is the emission from the active galactic nucleus.

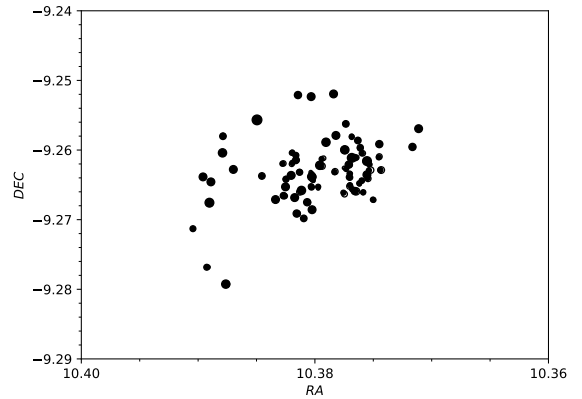


Figure 7. The scatter plot of knots detected from NUV (filled circle) and H α image (open circle). The knots detected from NUV and H α images are not displaying any offset.

of the star formation rate of the knots is shown in Figure 11. We note that the star formation rate is high on the disk of the galaxy and generally low over the star forming knots in the intergalactic medium.

We estimate the integrated star formation rate from FUV to be $\sim 15 M_{\odot}/yr$. We also calculate the star formation rate of the NUV detected knots from the measured H α flux within the knots using the formalism described in Kennicutt (1998) and shown below.

$$SFR_{H\alpha}[M_{\odot}/yr] = 7.9 \times 10^{-42} \times L_{H\alpha}[erg/sec] \quad (2)$$

The integrated star formation rate from the H α emission within the NUV-detected knots is found to be $\sim 10 M_{\odot}/yr$. We compared the SFR derived from FUV and H α of the in-

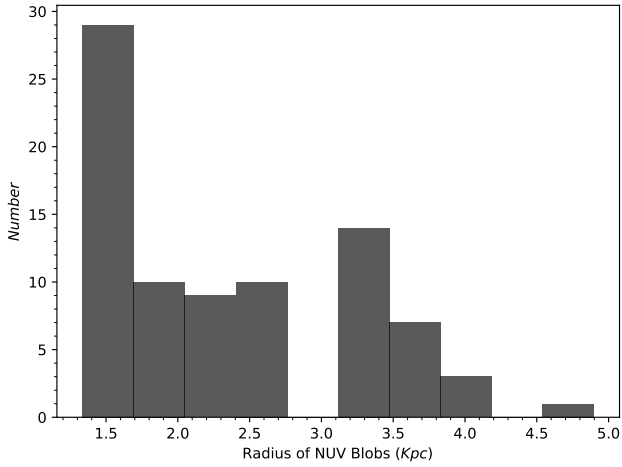


Figure 8. The histogram of the radius of the star forming knots detected from the NUV image of Jo201. The spatial resolution for the NUV image of JO201 is 1.3 *Kpc*.

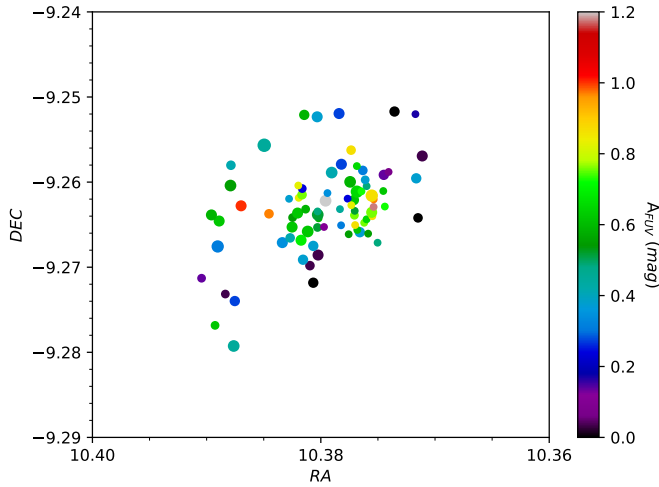


Figure 9. The distribution of the FUV extinction values (A_{FUV}) of the knots as projected in the sky coordinate (J2000). The points are color coded for the A_{FUV} as shown in the color bar and the size of the point is proportional to the radius of the knot.

dividual knots in Figure 12. The SFR of knots derived from the FUV and from $H\alpha$ agree remarkably well. The values uncorrected for dust follow very closely the 1:1 relation (black points); when they are corrected for dust (red points), the UV-based SFR are slightly larger than those derived from $H\alpha$. This was calculated assuming a stellar over gas $E(B-V)$ value of 0.44 as in the standard Calzetti's formulation, while using a value of 0.32 the two estimates would follow the 1:1 relation. This might suggest that in the knots in jellyfish galaxies the difference between the extinction affecting the stellar light and the extinction of the youngest, most massive stars producing the ionizing radiation is even larger than in

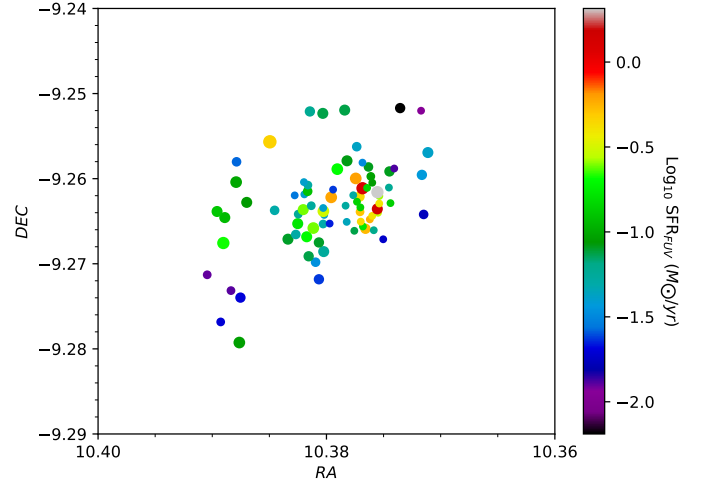


Figure 10. The distribution of the star formation rates of the star forming knots projected in the sky coordinate (J2000). The points are color coded for the $\log_{10}(\text{SFR})$ as shown in the color bar and the size of the point is proportional to the radius of the knot.

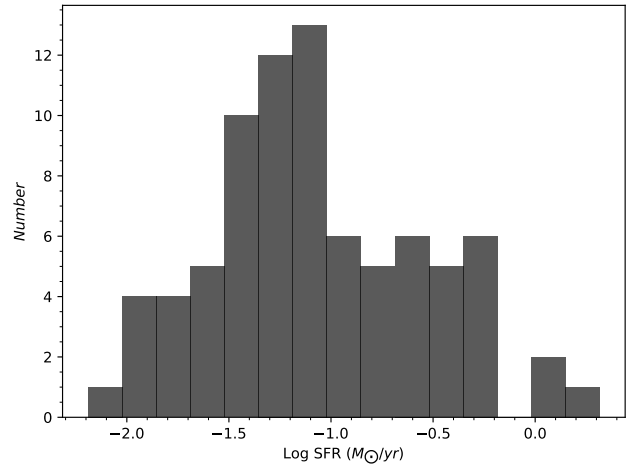


Figure 11. The histogram of the star formation rates computed using the measured FUV flux of the star forming knots. Note that the star forming knots have a range in star formation rates.

the average starburst local galaxies studied by Calzetti et al. (2000).

It is important to keep in mind that the star formation rates are obtained based on assumptions that are affected by large uncertainties, most importantly the shape of the IMF and the recent star formation history (bursty, continuous, or over what timescale). The star formation rate calculation is calibrated for galaxies which have ongoing star formation in the disk of the galaxy (Kennicutt 1998), while the jellyfish galaxy studied here is having star formation in a different environment. The estimates given above must therefore be taken with caution and considering all the possible caveats.

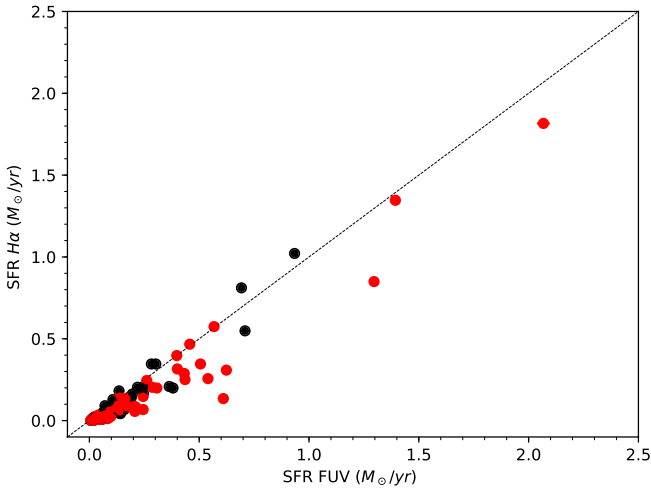


Figure 12. The SFR derived from FUV flux is compared against the SFR derived from $H\alpha$ flux for the 80 knots. The black points correspond to SFR derived with no extinction correction applied and the red points correspond to SFR with extinction correction applied to FUV and $H\alpha$ flux values.

4 DISCUSSION

The star formation in the ram-pressure stripped tails of a few galaxies was studied at UV wavelengths using GALEX (Chung et al. 2009; Smith et al. 2010; Hester et al. 2010; Fumagalli et al. 2011; Kenney et al. 2014). The ultraviolet observation of JO201 in the Abell 85 galaxy cluster reveals a wealth of information on the ongoing star formation in a jellyfish galaxy. We detect star forming knots both on the galaxy disk and outside of the galaxy hanging in the intergalactic space. We are observing the triggered star formation in the gas that got stripped from the galaxy due to the impact of galaxy infall onto the hot intra cluster medium. The UV observations presented in this paper provide strong evidence for ongoing star formation in the ram pressure stripped gas of JO201. The knots of star formation detected from UV imaging are found to have significant $H\alpha$ flux. This supports the notion that the UV and $H\alpha$ flux of the knots are having a single origin and that is ongoing star formation.

We note that the peak emission of knots in UV and $H\alpha$ images show very good correspondence in position. The offset seen in previous studies between the $H\alpha$ and UV emission of the knots is not seen in the present study. This can be due to the orientation at which the galaxy JO201 is falling into the cluster. As discussed in Bellhouse et al. (2017), the jellyfish galaxy JO201 is falling from the backside of the cluster with a slight inclination to the line-of-sight directed to the west. The projection of the knots along the line-of-sight may inhibit any offset between $H\alpha$ and UV emission from the knots. Alternatively a lack of offset is intrinsic in nature to this jellyfish which can be dependent on the time scales involved in the stripping of gas from the galaxy and the onset of star burst in the knots. A statistical analysis of

more jellyfish galaxies in UV and $H\alpha$ is therefore needed to understand more details on the stellar emission regions.

The star formation rate of the star forming knots is showing higher values on the galaxy disk (particular at the north western region) of JO201 compared to knots outside the disk in the intergalactic medium. The enhanced star formation rate on the disk can be interpreted as due to the trajectory of the galaxy falling into the Abell 85 galaxy cluster. JO201 is falling into the cluster from the back with a slight inclination from the line-of-sight directed to the west (Bellhouse et al. 2017; Jaffe' et al. 2018). The galaxy could be considered as freshly acquired from the field and might be undergoing the first infall into the Abell 85 galaxy cluster. The enhanced star formation rate region (north western region) can be undergoing the first contact point of galaxy and the hot intra-cluster medium of Abell 85.

We found that the flux in the knots when not corrected for extinction at the source, yields a good agreement between the derived SFR_{FUV} and $SFR_{H\alpha}$ values as shown in Figure 12. This remarkably tight correlation deviates slightly more from the 1:1 relation (particular at lower values and for knots outside the disk of galaxy) when the correction for extinction is applied, possibly suggesting that the average dust extinction assumptions commonly used for local starburst galaxies do not apply to these systems.

The integrated SFR for JO201 derived from the FUV flux ($SFR_{FUV} \sim 15 M_{\odot}/yr$) is found to be rather typical for normal star forming galaxies of this mass in the local Universe. The specific star formation rate (SSFR) of JO201 is calculated to be $10^{-9.6} yr^{-1}$ and falls on the star formation main sequence in the SSFR vs stellar mass plot of star forming galaxies in the local Universe (Salim et al. 2007).

Finally we note that the UV study of jellyfish galaxy JO201 presented here can be considered as a bench mark for observing higher redshift jellyfish galaxies using big optical telescopes. The rest frame UV emission will then be redshifted to optical wavelengths. The clumpy star formation in the intergalactic medium can also be speculated to be similar in nature during the peak of star formation epochs at $z > 2$. The study of such systems in UV in the local Universe can give more insights into the triggered star formation in dense environments.

5 SUMMARY

We have studied star formation in the jellyfish galaxy JO201 (taken from GASP sample) using the ultraviolet imaging observation from UVIT. Intense star formation is seen in the tentacles and disk of the galaxy. We compared the FUV/NUV imaging data with the $H\alpha$ imaging data of JO201 and following inferences are made.

- The tentacles and main body of the jellyfish galaxy show strong UV emission. The emitting regions in UV and $H\alpha$ are showing remarkable correlation. $H\alpha$ emission is originating from the hot ionized HII regions surrounding the young OB stars, where as UV is coming directly from the photospheres of OBA stars. We confirm that both (UV and $H\alpha$) are having the same origin and that is ongoing star formation.
- We search for a possible (physically motivated) spatial offset between the UV and $H\alpha$ emission from the detected

knots, but could not detect any offset above the instrument resolution.

- We detected and confirmed 80 star forming knots on the disk and tentacles of galaxy JO201 from the NUV imaging data. The FUV extinction for the knots are computed making use of the A_V values derived from the Balmer decrement.

- The star formation rates of individual knots are derived from the extinction corrected FUV flux and found to range from ~ 0.01 to $2.07 M_{\odot} \text{ yr}^{-1}$. We show that the star formation rate of the knots derived from FUV flux agree very well with the ones derived from $H\alpha$ flux.

- The integrated star formation rate for JO201 derived from FUV is $\sim 15 M_{\odot} \text{ yr}^{-1}$ and is shown to be comparable to star forming galaxies of similar mass range in the local Universe.

- We demonstrate that our unprecedented deep UV imaging study of the jellyfish galaxy JO201 show clear signs of extraplanar star-formation activity, resulting from a recent/ongoing gas stripping event.

The study of JO201 like systems in UV in the local Universe can give more insights into the triggered star formation in dense environments at high redshifts.

ACKNOWLEDGEMENTS

This publication uses the data from the AstroSat mission of the Indian Space Research Organisation (ISRO), archived at the Indian Space Science Data Centre (ISSDC). UVIT project is a result of collaboration between IIA, Bengaluru, IUCAA, Pune, TIFR, Mumbai, several centres of ISRO, and CSA. Based on observations collected by the European Organisation for Astronomical Research in the Southern Hemisphere under ESO program 196.B-0578 (MUSE). We acknowledge financial support from PRIN-SKA 2017. B.V. acknowledges the support from an Australian Research Council Discovery Early Career Researcher Award (PD0028506). This research made use of Astropy, a community-developed core Python package for Astronomy ([The Astropy Collaboration et al. 2018](#)).

REFERENCES

Agrawal, P. C. 2006, *Advances in Space Research*, 38, 2989
The Astropy Collaboration, Price-Whelan, A. M., Sipőcz, B. M., et al. 2018, [arXiv:1801.02634](#)
Baldry, I. K., Glazebrook, K., Brinkmann, J., et al. 2004, *ApJ*, 600, 681
Bekki, K. 2009, *MNRAS*, 399, 2221
Bellhouse, C., Jaffé, Y. L., Hau, G. K. T., et al. 2017, *ApJ*, 844, 49
Butcher, H., & Oemler, A., Jr. 1984, *ApJ*, 285, 426
Calzetti, D., Armus, L., Bohlin, R. C., et al. 2000, *ApJ*, 533, 682
Cardelli, J. A., Clayton, G. C., & Mathis, J. S. 1989, *ApJ*, 345, 245
Cayatte, V., van Gorkom, J. H., Balkowski, C., & Kotanyi, C. 1990, *AJ*, 100, 604
Chabrier, G. 2003, *PASP*, 115, 763
Chung, A., van Gorkom, J. H., Kenney, J. D. P., Crowl, H., & Vollmer, B. 2009, *AJ*, 138, 1741
Cortese, L., Marzicall, D., Richard, J., et al. 2007, *MNRAS*, 376, 157

Cortese, L., Gavazzi, G., & Boselli, A. 2008, *MNRAS*, 390, 1282
Dressler, A. 1980, *ApJ*, 236, 351
Dressler, A., Oemler, A., Jr., Couch, W. J., et al. 1997, *ApJ*, 490, 577
Dressler, A., Oemler, A., Jr., Poggianti, B. M., et al. 2013, *ApJ*, 770, 62
Ebeling, H., Stephenson, L. N., & Edge, A. C. 2014, *ApJ*, 781, L40
Fabian, A. C. 1994, *ARA&A*, 32, 277
Fasano, G., Marmo, C., Varela, J., et al. 2006, *A&A*, 445, 805
Fasano, G., Poggianti, B. M., Bettoni, D., et al. 2015, *MNRAS*, 449, 3927
Fumagalli, M., Gavazzi, G., Scaramella, R., & Franzetti, P. 2011, *A&A*, 528, A46
Fumagalli, M., Fossati, M., Hau, G. K. T., et al. 2014, *MNRAS*, 445, 4335
Girish, V., Tandon, S. N., Sriram, S., Kumar, A., & Postma, J. 2017, *Experimental Astronomy*, 43, 59
Gullieuszik, M., Poggianti, B., Fasano, G., et al. 2015, *A&A*, 581, A41
Gullieuszik, M., Poggianti, B. M., Moretti, A., et al. 2017, *ApJ*, 846, 27
Gunn, J. E., & Gott, J. R., III 1972, *ApJ*, 176, 1
Haynes, M. P., Giovanelli, R., & Chincarini, G. L. 1984, *ARA&A*, 22, 445
Hester, J. A., Seibert, M., Neill, J. D., et al. 2010, *ApJ*, 716, L14
Iglesias-Páramo, J., Buat, V., Takeuchi, T. T., et al. 2006, *ApJS*, 164, 38
Jáchym, P., Sun, M., Kenney, J. D. P., et al. 2017, *ApJ*, 839, 114
Jáchym, P., Combes, F., Cortese, L., Sun, M., & Kenney, J. D. P. 2014, *ApJ*, 792, 11
Jaffé, Y. L., Smith, R., Candlish, G. N., et al. 2015, *MNRAS*, 448, 1715
Jaffe', Y. L., Poggianti, B. M., Moretti, A., et al. 2018, [arXiv:1802.07297](#)
Kenney, J. D. P., & Koopmann, R. A. 1999, *AJ*, 117, 181
Kenney, J. D. P., van Gorkom, J. H., & Vollmer, B. 2004, *AJ*, 127, 3361
Kenney, J. D. P., Geha, M., Jáchym, P., et al. 2014, *ApJ*, 780, 119
Kennicutt, R. C., Jr. 1998, *ARA&A*, 36, 189
Kennicutt, R. C., & Evans, N. J. 2012, *ARA&A*, 50, 531
Kumar, A., Ghosh, S. K., Hutchings, J., et al. 2012, *Proc. SPIE*, 8443, 84431N
Lang, D., Hogg, D. W., Mierle, K., Blanton, M., & Roweis, S. 2010, *AJ*, 139, 1782
Leitherer, C., Schaerer, D., Goldader, J. D., et al. 1999, *ApJS*, 123, 3
López-Sánchez, Á. R., Westmeier, T., Esteban, C., & Koribalski, B. S. 2015, *MNRAS*, 450, 3381
Madau, P., Pozzetti, L., & Dickinson, M. 1998, *ApJ*, 498, 106
Madau, P., & Dickinson, M. 2014, *ARA&A*, 52, 415
Mahajan, S., Raychaudhury, S., & Pimblett, K. A. 2012, *MNRAS*, 427, 1252
Moretti, A., Gullieuszik, M., Poggianti, B., et al. 2017, *A&A*, 599, A81
Oemler, A., Jr., Dressler, A., Kelson, D., et al. 2009, *ApJ*, 693, 152-173
Owen, F. N., Keel, W. C., Wang, Q. D., Ledlow, M. J., & Morrison, G. E. 2006, *AJ*, 131, 1974
Owers, M. S., Couch, W. J., Nulsen, P. E. J., & Randall, S. W. 2012, *ApJ*, 750, L23
Poggianti, B. M., Smail, I., Dressler, A., et al. 1999, *ApJ*, 518, 576
Poggianti, B. M., Fasano, G., Omizzolo, A., et al. 2016, *AJ*, 151, 78
Poggianti, B. M., Moretti, A., Gullieuszik, M., et al. 2017, *ApJ*, 844, 48

- Poggianti, B. M., Jaffé, Y. L., Moretti, A., et al. 2017, *Nature*, 548, 304
- Postma, J. E., & Leahy, D. 2017, *PASP*, 129, 115002
- Rawle, T. D., Altieri, B., Egami, E., et al. 2014, *MNRAS*, 442, 196
- Salim, S., Rich, R. M., Charlot, S., et al. 2007, *ApJS*, 173, 267
- Salpeter, E. E. 1955, *ApJ*, 121, 161
- Sarazin, C. L. 1986, *Reviews of Modern Physics*, 58, 1
- Serra, P., Koribalski, B., Duc, P.-A., et al. 2013, *MNRAS*, 428, 370
- Shull, J. M., & McKee, C. F. 1979, *ApJ*, 227, 131
- Smith, R. J., Lucey, J. R., Hammer, D., et al. 2010, *MNRAS*, 408, 1417
- Subramaniam, A., Tandon, S. N., Hutchings, J., et al. 2016, *Proc. SPIE*, 9905, 99051F
- Tandon, S. N., Hutchings, J. B., Ghosh, S. K., et al. 2016, *arXiv:1612.00612*
- Tandon, S. N., Subramaniam, A., Girish, V., et al. 2017, *arXiv:1705.03715*
- Tonnesen, S., & Bryan, G. L. 2009, *ApJ*, 694, 789
- Tonnesen, S., & Bryan, G. L. 2012, *MNRAS*, 422, 1609
- Varela, J., D’Onofrio, M., Marmo, C., et al. 2009, *A&A*, 497, 667
- Venkatapathy, Y., Bravo-Alfaro, H., Mayya, Y. D., et al. 2017, *AJ*, 154, 227
- Verdugo, C., Combes, F., Dasyra, K., Salomé, P., & Braine, J. 2015, *A&A*, 582, A6
- Visvanathan, N., & Sandage, A. 1977, *ApJ*, 216, 214
- Vollmer, B., Cayatte, V., Balkowski, C., & Duschl, W. J. 2001, *ApJ*, 561, 708
- Yoon, H., Chung, A., Smith, R., & Jaffé, Y. L. 2017, *ApJ*, 838, 81
- Yoshida, M., Yagi, M., Komiyama, Y., et al. 2008, *ApJ*, 688, 918–930

This paper has been typeset from a \LaTeX file prepared by the author.